Canonical transforms and the efficient integration of quantum mechanical wave equations

Heiko Bauke* and Christoph H. Keitel†
Max-Planck-Institut für Kernphysik, Saupfercheckweg 1, 69117 Heidelberg, Germany
(Received 27 April 2009; published 23 July 2009)

The integration of time-dependent quantum mechanical wave equations is a fundamental problem in computational physics and computational chemistry. The wave-function's energy spectrum as well as its momentum spectrum impose fundamental limits on the performance of numerical algorithms for the solution of wave equations. We demonstrate how canonical transforms may be applied to negotiate these limitations and to increase the performance of numerical algorithms by up to several orders of magnitude. Our approach includes the so-called Kramers-Henneberger transform as a special case and puts forward modifications toward an improved numerical efficiency.

DOI: 10.1103/PhysRevE.80.016706 PACS number(s): 02.70.−c, 03.65.−w

I. INTRODUCTION

The time-spatial evolution of quantum mechanical systems is determined by quantum wave equations, e.g., the Schrödinger equation, the Pauli equation, or its relativistic analog the Dirac equation. Analytic solutions to these equations are known for only a few systems [1,2] and, therefore, numerical algorithms are an indispensable tool for the theoretical investigation of quantum mechanical systems. In fact, numerical approaches to the Schrödinger equation had been undertaken long before electronic calculating machines became available [3].

Various authors have proposed different algorithms for an efficient solution of quantum mechanical wave equations during the last decades. Among the most popular methods are the Crank-Nicolson scheme [4–6], the leap-frog method [7,8], and the split operator method [9]. In order to increase its efficiency, generalizations to higher orders of accuracy have been suggested for the Crank-Nicolson scheme [10], the leap-frog method [11], as well as for the split operator method [12–15]. Recent approaches to solve quantum wave equations include, for example, the real-space-product finite-element discrete-variable representation approach [16–18], Chebychev propagator methods [19], and the quantum lattice Boltzmann method [20–22]. Initially, the algorithms mentioned above have been introduced to solve the time-dependent Schrödinger equation and a comparison of various numerical integration schemes for this equation can be found in [23]. However, these methods can also be applied to relativistic quantum mechanical wave equations [24–26].

In contrast to [4–26] and many other publications that deal with the efficient integration of quantum mechanical wave equations, we are not trying to deduce another actual numerical scheme. Instead, we will show that the choice of the Hilbert-space representation of a quantum mechanical system has a crucial impact on the efficiency of numerical algorithms and we will demonstrate how a reformulation of the wave equation by means of a canonical transform can increase both the performance and the accuracy of existing algorithms significantly.

*bauke@mpi-hd.mpg.de
†keitel@mpi-hd.mpg.de

This paper is organized as follows. After a short review of quantum mechanical wave equations in Sec. II, we will draw the reader's attention in Sec. III to some fundamental limits that are related to the numerical solution of quantum wave equations. In Secs. V and VI we will introduce some techniques that allow us to negotiate these limitations by translating the Hamiltonian by canonical transforms. Canonical transforms will be reviewed in Sec. IV. Finally, Sec. VII presents some numerical results and benchmarks.

II. QUANTUM MECHANICAL WAVE EQUATIONS

The state of a quantum mechanical system is specified by a wave function $\Psi(\boldsymbol{x},t)$. This function spreads continuously in time t and space $\boldsymbol{x}$; its evolution is governed by a quantum mechanical wave equation that has a so-called Schrödinger form

$$i\hbar\frac{\partial}{\partial t}\Psi(\boldsymbol{x},t)=\hat{H}\Psi(\boldsymbol{x},t) \tag{1}$$

or can be transformed into this form, where $\hbar$ denotes the Planck constant divided by 2π. Equation (1) includes various wave equations that share the same mathematical structure, e.g., the Schrödinger equation, the Pauli equation, the Dirac equation [27], as well as the Klein-Gordon equation in the Feshbach-Villars representation [28]. However, the form of the wave function $\Psi(\boldsymbol{x},t)$ and the operator $\hat{H}$ (the Hamiltonian) differs.

The Schrödinger equation is an equation for a complex-valued scalar wave function $\Psi(\boldsymbol{x},t)$. In its most general form, it describes a particle of mass m and charge q in the electromagnetic potentials $\phi(\boldsymbol{x},t)$ and $\boldsymbol{A}(\boldsymbol{x},t)$. The Schrödinger equation Hamiltonian reads as

$$\hat{H}=\frac{1}{2m}\left(-i\hbar\frac{\partial}{\partial\boldsymbol{x}}-q\boldsymbol{A}(\boldsymbol{x},t)\right)^2+q\phi(\boldsymbol{x},t). \tag{2}$$

It describes a nonrelativistic spin zero particle and is invariant under the Galilean transformation. In contrast to the Schrödinger equation, the Dirac equation describes a relativistic spin half particle and is invariant under the Lorentz transformation. Its Hamiltonian is given by

$$\hat{H} = c\boldsymbol{\alpha}\cdot\left(-i\hbar\frac{\partial}{\partial \boldsymbol{x}} - q\boldsymbol{A}(\boldsymbol{r},t)\right) + q\phi(\boldsymbol{r},t) + mc^2\beta, \quad (3)$$

with $\boldsymbol{\alpha}=(\alpha_1,\alpha_2,\alpha_3)^{\mathrm{T}}$ and the speed of light c. The 4×4 matrices $\alpha_1,\alpha_2,\alpha_3$, β obey the algebra

$$\alpha_i^2 = \beta^2 = 1, \quad \alpha_i\alpha_k + \alpha_k\alpha_i = 2\delta_{i,k}, \quad \alpha_i\beta + \beta\alpha_i = 0, \quad (4)$$

with $i,k\in\{1,2,3\}$. A Dirac wave function is a four component complex-valued vector function. For one-dimensional systems, the Dirac wave function reduces to a two component complex-valued vector function and the matrices α_1 and β reduce to 2×2 matrices.

In the subsequent sections, we are going to formulate our arguments as generically as possible. That means we will use the fact that wave equations are given in Schrödinger form (1), but we will not take into account specific features of particular Hamiltonians. However, for illustrative purposes and in numerical applications, we will refer to the Schrödinger equation (2) and the Dirac equation (3).

III. FUNDAMENTAL LIMITS OF NUMERICAL ALGORITHMS

Quantum mechanical wave functions $\Psi(\boldsymbol{x},t)$ spread continuously in time and space. Every numerical algorithm for the propagation of a wave function (that works in real space) will reconstruct the wave function on discrete points in time and space starting from an initial condition $\Psi(\boldsymbol{x},0)=\Psi_0(\boldsymbol{x})$. For simplicity, let us assume that the spacing of these points is equidistant and given by Δx for spatial dimensions and by Δt for the temporal dimension. When propagating $\Psi(\boldsymbol{x},t)$ over a fixed domain in time and space, it is desirable to render the number of space-time sampling points small, that is, to make Δt and Δx large because the computing time grows with the number of space-time sampling points. Yet, Δt and Δx cannot be chosen arbitrarily large.

They are limited not only by algorithm specific constraints. In fact, the magnitude of the wave-function's time-spatial oscillations restricts Δt and Δx in a fundamental way. The energy and the canonical momentum operators in coordinate representation are proportional to derivatives with respect to time and space, respectively. Therefore, temporal oscillations of $\Psi(\boldsymbol{x},t)$ are related to the energy spectrum, while spatial oscillations are related to the momentum spectrum of the quantum mechanical system. The Shannon sampling theorem [29] establishes a relation between spatial oscillations and Δx and temporal oscillations and Δt more rigorously. It imposes *fundamental* limits on Δx and Δt.

Let us consider a one-dimensional system with a time-independent Hamiltonian $\hat{H}$ and a wave function $\Psi(x,t)$ in its coordinate representation. The wave function can be expanded into various bases, e.g., into eigenfunctions $\Psi_E(x)$ of the Hamiltonian $\hat{H}$ or into plane waves $\exp[i(px-E(p)t)/\hbar]$, where $E(p)$ denotes the energy-momentum relation of a free particle with mass m; $E(p)=p^2/(2m)$ for Galilean invariant wave equations and $E(p)=\sqrt{m^2c^4+p^2c^2}$ for Lorentz invariant wave equations, respectively. If $\Psi(x,t)$ is band limited in the momentum domain to $\tilde{p}$ and band limited in the energy domain to $\tilde{E}$, respectively, then the expansion of $\Psi(x,t)$ into plane waves reads as

$$\Psi(x,t) = \int_{-\tilde{p}}^{\tilde{p}} a(p,t)\exp\left(-\frac{i}{\hbar}E(p)t\right)\exp\left(\frac{i}{\hbar}px\right)dp \quad (5a)$$

and the expansion into energy eigenfunctions is given by

$$\Psi(x,t) = \int_{-\tilde{E}}^{\tilde{E}} b(E)\Psi_E(x)\exp\left(-\frac{i}{\hbar}Et\right)dE. \quad (5b)$$

We call $\tilde{p}$ as the momentum band limit and $\tilde{E}$ as the energy band limit of the system.

The Shannon sampling theorem states that $\Psi(x,t)$ can be reconstructed from evenly distributed sampling points if and only if

$$\Delta x \le \frac{\hbar\pi}{\tilde{p}}, \quad \Delta t \le \frac{\hbar\pi}{\tilde{E}}. \quad (6)$$

Note that Eq. (6) is a necessary constraint on the step sizes Δx and Δt. Practical numerical algorithms may require considerably smaller step sizes, e.g., because of algorithm specific instabilities [30,31].

IV. CANONICAL TRANSFORMS

A (quantum) canonical transform (Table I) is a change in phase-space variables from $(\hat{\boldsymbol{x}},\hat{\boldsymbol{p}})$ to $(\hat{\boldsymbol{x}}',\hat{\boldsymbol{p}}')$ that preserves the canonical commutation relation,

$$\hat{\boldsymbol{x}}\hat{\boldsymbol{p}} - \hat{\boldsymbol{p}}\hat{\boldsymbol{x}} = \hat{\boldsymbol{x}}'\hat{\boldsymbol{p}}' - \hat{\boldsymbol{p}}'\hat{\boldsymbol{x}}' = i\hbar. \quad (7)$$

Canonical transforms played a prominent role in the conceptual development of quantum mechanics [32,33] and have proven to be a valuable tool for the analytical treatment of quantum mechanical problems. In this contribution, we will demonstrate how canonical transforms can help to overcome the fundamental limitation of numerical algorithms (6).

Let $\hat{O}$ be a Hermitian operator that represents some observable with a possibly time-dependent expectation value

$$\langle O\rangle(t) = \int \overline{\Psi(\boldsymbol{x},t)}\hat{O}\Psi(\boldsymbol{x},t)d^3x \quad (8)$$

and $\hat{U}$ a unitary transform. Then the mapping of $\hat{O}$ to

$$\hat{O}' = \hat{U}\hat{O}\hat{U}^{-1} \quad (9)$$

is a canonical transform. Both $\hat{O}$ and $\hat{O}'$ have the same eigenvalue spectra—the same expectation values—that is, $\langle O\rangle(t)=\langle O'\rangle(t)$, and represent the same observable in different Hilbert spaces $\mathcal{H}$ and $\mathcal{H}'$. In each Hilbert space there exists a wave function that encodes the evolution of the same quantum mechanical system. Let the wave function $\Psi(\boldsymbol{x},t)$ evolve in $\mathcal{H}$ under Eq. (1) then the evolution of $\Psi'(\boldsymbol{x},t)$ in $\mathcal{H}'$ is determined by

$$\hat{U}i\hbar\frac{\partial}{\partial t}\hat{U}^{-1}\Psi'(\boldsymbol{x},t) = \hat{U}\hat{H}\hat{U}^{-1}\Psi'(\boldsymbol{x},t). \quad (10)$$

From Eqs. (1) and (10), it follows that $\Psi(\boldsymbol{x},t)$ and $\Psi'(\boldsymbol{x},t)$ are related by

TABLE I. Operators of some observables in coordinate representation and their representation after a canonical transform $\Psi'(\boldsymbol{x},t)=\hat{U}\Psi(\boldsymbol{x},t)$. There are two different ways to interpret the new wave function $\Psi'(\boldsymbol{x},t)$. Either it represents the same physical system as $\Psi(\boldsymbol{x},t)$ does but in another Hilbert space where operators of observables have a nonstandard representation or $\Psi'(\boldsymbol{x},t)$ represents a new system with Hamiltonian $\hat{H}^*$, where operators are given in standard representation.

	Original system in standard coordinate representation	Original system in transformed representation	New system in coordinate representation
Position	$\hat{\boldsymbol{x}}=\boldsymbol{x}$	$\hat{\boldsymbol{x}}'=\hat{U}\boldsymbol{x}\hat{U}^{-1}$	$\hat{\boldsymbol{x}}^*=\boldsymbol{x}$
Momentum	$\hat{\boldsymbol{p}}=-i\hbar\frac{\partial}{\partial \boldsymbol{x}}$	$\hat{\boldsymbol{p}}'=\hat{U}(-i\hbar\frac{\partial}{\partial \boldsymbol{x}})\hat{U}^{-1}$	$\hat{\boldsymbol{p}}^*=-i\hbar\frac{\partial}{\partial \boldsymbol{x}}$
Energy	$\hat{E}=i\hbar\frac{\partial}{\partial t}$	$\hat{E}'=\hat{U}(i\hbar\frac{\partial}{\partial t})\hat{U}^{-1}$	$\hat{E}^*=i\hbar\frac{\partial}{\partial t}$
Hamiltonian	$\hat{H}$	$\hat{H}'=\hat{U}\hat{H}\hat{U}^{-1}$	$\hat{H}^*=\hat{U}\hat{H}\hat{U}^{-1}-\hat{U}(i\hbar\frac{\partial}{\partial t}\hat{U}^{-1})$

$$\Psi'(\boldsymbol{x},t)=\hat{U}\Psi(\boldsymbol{x},t). \tag{11}$$

To construe $\Psi(\boldsymbol{x},t)$ and $\Psi'(\boldsymbol{x},t)$ as wave functions for the *same physical system* in different Hilbert spaces is not the only possible interpretation of the mapping (11). As we pointed out in Sec. III, the limits (6) have their roots in the coordinate representation of the energy operator and the canonical momentum operator. If one maintains the standard coordinate representation of the position operator, the momentum operator, the energy operator, and other operators then $\Psi'(\boldsymbol{x},t)$ can be interpreted as the wave function of a *new system* with a new Hamiltonian $\hat{H}^*$. Solving Eq. (10) for $i\hbar\frac{\partial}{\partial t}\Psi'(\boldsymbol{x},t)$, we find the Schrödinger form $i\hbar\frac{\partial}{\partial t}\Psi'(\boldsymbol{x},t)=\hat{H}^*\Psi'(\boldsymbol{x},t)$ with

$$\hat{H}^*=\hat{U}\hat{H}\hat{U}^{-1}-\hat{U}\left(i\hbar\frac{\partial}{\partial t}\hat{U}^{-1}\right). \tag{12}$$

In the reminder of the paper and if not stated otherwise, we refer to the stared operators as shown in Table I if we speak of the Hamiltonian, the momentum operator, the energy operator, etc., of the new wave function $\Psi'(\boldsymbol{x},t)$.

In general, the energy and canonical momentum spectra of the new system will differ from the ones of the original system. In particular, the expectation value of the energy $\langle E\rangle(t)$ is shifted to

$$\langle E'\rangle(t)=\langle E\rangle(t)+i\hbar\int\overline{\hat{U}\Psi(\boldsymbol{x},t)}\frac{\partial\hat{U}}{\partial t}\Psi(\boldsymbol{x},t)d^3x. \tag{13}$$

For the expectation value of the momentum $\langle\boldsymbol{p}\rangle(t)$, we find the analogous result

$$\langle\boldsymbol{p}'\rangle(t)=\langle\boldsymbol{p}\rangle(t)-i\hbar\int\overline{\hat{U}\Psi(\boldsymbol{x},t)}\frac{\partial\hat{U}}{\partial \boldsymbol{x}}\Psi(\boldsymbol{x},t)d^3x. \tag{14}$$

This modification of the energy and momentum spectra is the key to efficient numerical algorithms for the integration of quantum mechanical wave equations and we will seek for phase-space transforms $\hat{U}$ leading to Hamiltonians $\hat{H}^*$ that are more convenient for numerical algorithms than $\hat{H}$. In order to overcome the limits enforced by the Shannon sampling theorem, the transform $\hat{U}$ will be chosen in a way such that $\Psi'(\boldsymbol{x},t)$ has a smaller band limit in the momentum domain and/or a smaller band limit in the energy domain than $\Psi(\boldsymbol{x},t)$. Hence, $\Psi'(\boldsymbol{x},t)$ will less fluctuate in space and/or in time.

The transition from the Schrödinger picture to the Heisenberg picture is an important example for the type of transforms we are looking for. Using Dyson's time-ordering operator $\hat{T}$, the temporal evolution of an initial wave function $\Psi(\boldsymbol{x},0)$ under the effect of the Hamiltonian $\hat{H}$ is determined by a unitary operator $\hat{U}_{\hat{H}}$,

$$\Psi(\boldsymbol{x},t)=\hat{U}_{\hat{H}}\Psi(\boldsymbol{x},0), \tag{15a}$$

with

$$\hat{U}_{\hat{H}}=\hat{T}\exp\left(-\frac{i}{\hbar}\int_0^t\hat{H}(\tau)d\tau\right). \tag{15b}$$

The operator $\hat{U}_{\hat{H}}^{-1}$ establishes the transition from the Schrödinger picture to the Heisenberg picture. In the Schrödinger picture, the wave function evolves in time; position and momentum operators are time independent. In the Heisenberg picture, however, position and momentum operators are time dependent but the wave function does not depend on time,

$$i\hbar\frac{\partial}{\partial t}\Psi'(\boldsymbol{x},t)=i\hbar\frac{\partial}{\partial t}\hat{U}_{\hat{H}}^{-1}\Psi(\boldsymbol{x},t)=i\hbar\frac{\partial}{\partial t}\Psi(\boldsymbol{x},0)=0. \tag{16}$$

Therefore, $\hat{U}_{\hat{H}}^{-1}$ provides a transform that allows numerical algorithms to take arbitrary large time steps Δt. However, calculating $\hat{U}_{\hat{H}}^{-1}$ is as difficult as calculating the evolution of $\Psi(\boldsymbol{x},t)$. As we will show in the following sections, there are other more applicatory canonical transforms that reduce temporal and/or spatial fluctuations of the wave function.

One should note that the idea of using phase-space transformations to overcome limitations imposed on the efficiency of specific numeric integration algorithms has been implemented earlier, e.g., in molecular-dynamics simulations of classical systems [34] by splitting algorithms. However, here we take a broader perspective; our arguments do not make any algorithm specific assumptions. The phase-space transformations that we are looking for will be induced by

the physical properties of the system under investigation not by algorithm specific considerations.

V. GAUGE TRANSFORMS AND SPECTRUM-GUIDED INTEGRATION

In order to reduce a wave-function's high-frequency time-spatial oscillations, we propose a technique called *spectrum-guided integration* that is based on gauge transforms. Gauge transforms are canonical transforms, which are induced by a scalar gauge function $g(\boldsymbol{x},t)$ via

$$\hat{U}_g = \exp(ig(\boldsymbol{x},t)/\hbar). \tag{17}$$

Gauge transforms do not only preserve the canonical commutation relation (7), they also preserve the form of the quantum mechanical wave equation up to a change in the electromagnetic potentials, viz.,

$$\hat{H}^*(A'(\boldsymbol{x},t),\phi'(\boldsymbol{x},t)) = \hat{H}(A(\boldsymbol{x},t),\phi(\boldsymbol{x},t)), \tag{18}$$

with

$$\boldsymbol{A}'(\boldsymbol{x},t) = \boldsymbol{A}(\boldsymbol{x},t) + \frac{1}{q}\frac{\partial g(\boldsymbol{x},t)}{\partial \boldsymbol{x}}, \tag{19a}$$

$$\phi'(\boldsymbol{x},t) = \phi(\boldsymbol{x},t) - \frac{1}{q}\frac{\partial g(\boldsymbol{x},t)}{\partial t}. \tag{19b}$$

The electromagnetic fields $\boldsymbol{E}(\boldsymbol{x},t)$ and $\boldsymbol{B}(\boldsymbol{x},t)$ are invariant under gauge transforms

$$\begin{aligned}\boldsymbol{E}(\boldsymbol{x},t) &= -\frac{\partial\phi(\boldsymbol{x},t)}{\partial \boldsymbol{x}} - \frac{\partial \boldsymbol{A}(\boldsymbol{x},t)}{\partial t} \\ &= -\frac{\partial\phi'(\boldsymbol{x},t)}{\partial \boldsymbol{x}} - \frac{\partial \boldsymbol{A}'(\boldsymbol{x},t)}{\partial t} = \boldsymbol{E}'(\boldsymbol{x},t),\end{aligned} \tag{20a}$$

$$\boldsymbol{B}(\boldsymbol{x},t) = \frac{\partial}{\partial \boldsymbol{x}} \times \boldsymbol{A}(\boldsymbol{x},t) = \frac{\partial}{\partial \boldsymbol{x}} \times \boldsymbol{A}'(\boldsymbol{x},t) = \boldsymbol{B}'(\boldsymbol{x},t). \tag{20b}$$

Furthermore, gauge transforms preserve the probability density

$$\overline{\Psi(\boldsymbol{x},t)}\Psi(\boldsymbol{x},t) = \overline{\Psi'(\boldsymbol{x},t)}\Psi'(\boldsymbol{x},t) \tag{21}$$

and, as a consequence of Eq. (21), the center-of-mass motion is invariant under gauge transforms too,

$$\langle \boldsymbol{x}\rangle(t) = \langle \boldsymbol{x}'\rangle(t). \tag{22}$$

However, the expectation values of the energy as well as of the canonical momentum are shifted by gauge transforms. Using Eqs. (13) and (14), we find

$$\langle E'\rangle(t) = \langle E\rangle(t) - \langle g_t\rangle(t) \tag{23a}$$

and

$$\langle \boldsymbol{p}'\rangle(t) = \langle \boldsymbol{p}\rangle(t) + \langle g_{\boldsymbol{x}}\rangle(t), \tag{23b}$$

where we have introduced the quantities

$$\langle g_t\rangle(t) = \int \overline{\Psi(\boldsymbol{x},t)}\frac{\partial g(\boldsymbol{x},t)}{\partial t}\Psi(\boldsymbol{x},t)d^3x, \tag{24}$$

$$\langle g_{\boldsymbol{x}}\rangle(t) = \int \overline{\Psi(\boldsymbol{x},t)}\frac{\partial g(\boldsymbol{x},t)}{\partial \boldsymbol{x}}\Psi(\boldsymbol{x},t)d^3x. \tag{25}$$

The basic idea of the spectrum-guided integration is to reduce time-spatial oscillations by choosing a gauge function $g(\boldsymbol{x},t)$ such that the gauge transform causes a shift of the energy spectrum and/or the momentum spectrum so that $\langle E'\rangle(t)$ and/or $\langle \boldsymbol{p}'\rangle(t)$ vanish or are close to zero. That means the energy spectrum and/or the momentum spectrum are (approximately) centered around zero provided that the original energy and momentum spectra are not extremely skewed.

A. Reducing temporal oscillations

In order to reduce temporal oscillations by shifting the energy spectrum, we introduce a time-dependent gauge function,

$$g(\boldsymbol{x},t) = \int_0^t \bar{E}(\tau)d\tau, \tag{26}$$

that is parametrized by some function $\bar{E}(t)$. For this particular gauge transform, the new electromagnetic potentials (19) are given by

$$\boldsymbol{A}'(\boldsymbol{x},t) = \boldsymbol{A}(\boldsymbol{x},t), \tag{27a}$$

$$\phi'(\boldsymbol{x},t) = \phi(\boldsymbol{x},t) - \bar{E}(t)/q, \tag{27b}$$

and plugging Eq. (26) into Eqs. (23a) and (23b) we obtain the expectation values

$$\langle E'\rangle(t) = \langle E\rangle(t) - \bar{E}(t), \tag{28a}$$

$$\langle \boldsymbol{p}'\rangle(t) = \langle \boldsymbol{p}\rangle(t). \tag{28b}$$

We refer to the spectrum-guided integration in the *energy domain* if $\Psi(\boldsymbol{x},t)$ is transformed into $\Psi'(\boldsymbol{x},t)$ by a gauge transform (17) with Eq. (26) and $\bar{E}(t)$ such that the mean energy $\langle E'\rangle(t)$ of the new system $\Psi'(\boldsymbol{x},t)$ vanishes and for that reason $\Psi'(\boldsymbol{x},t)$ has a smaller energy band limit and exhibits temporal oscillations that have reduced frequencies compared to $\Psi(\boldsymbol{x},t)$.

For time-independent systems, $\langle E\rangle(t)$ is constant and may be computed from the initial condition; thus, we have $\bar{E}(t) = \langle E\rangle(t) = \langle \Psi(\boldsymbol{x},0)|\hat{H}|\Psi(\boldsymbol{x},0)\rangle$. In general, $\langle E\rangle(t)$ is not known *a priori*. However, if quantum effects are small, $\langle E\rangle(t)$ equals approximately the energy of the corresponding classical system. Therefore, we set $\bar{E}(t)$ to the energy of the classical system. Note that if $\bar{E}(t)$ does not strictly equal $\langle E\rangle(t)$, this just means that the reduction in the energy band limit might be nonoptimal, but this will not introduce any errors.

For one-dimensional wave functions, the effect of the gauge transform (26) may be visualized in two-dimensional

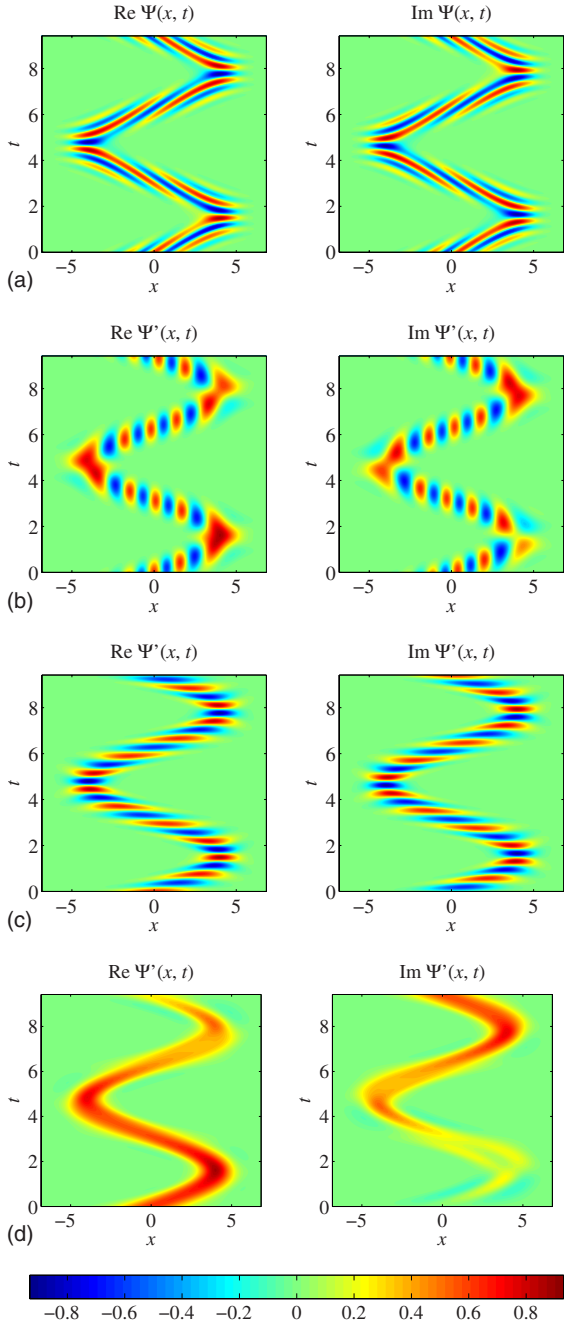

FIG. 1. (Color online) Reduction in time-spatial oscillations by the spectrum-guided integration. (a) A one-dimensional Gaussian wave packet $\Psi(x,t)$ in a harmonic potential with initial momentum $p=4$ and width $\sigma=1$ oscillates rapidly in time and space. (b) Spectrum-guided integration in the energy domain reduces temporal oscillations, while the (c) spectrum-guided integration in the momentum domain reduces spatial oscillations. (d) The combination of spectrum-guided integration in the energy domain and the spectrum-guided integration in the momentum domain smoothes the wave function and removes all fast oscillations. Figures display real (left) and imaginary (right) parts of the wave function.

diagrams that show the real and the imaginary parts of the wave function. Figure 1(a) shows the oscillation pattern of an initial Gaussian wave packet

$$\Psi(x,0) = \left(\frac{1}{2\pi\sigma^2}\right)^{1/4} \exp\left(-\frac{x^2}{4\sigma^2} + ipx\right), \tag{29}$$

with spatial width σ and momentum p evolving in a harmonic potential. The one-dimensional Schrödinger equation for a harmonic oscillator in dimensionless units with $\hbar=1$, $m=1$, and $q=1$ reads as

$$i\frac{\partial\Psi(x,t)}{\partial t} = -\frac{1}{2}\frac{\partial^2\Psi(x,t)}{\partial x^2} + \frac{x^2}{2}\Psi(x,t). \tag{30}$$

An analytic solution $\Psi(x,t)$ of the initial value problem given by (29) and (30) is presented in [35].

The wave function $\Psi(\boldsymbol{x},t)$ features high-frequency time-spatial oscillations as visualized in Fig. 1(a). However, temporal oscillations can be reduced by an appropriate gauge transform. The energy of a Gaussian wave packet (29) in a harmonic potential equals $\langle\Psi(x,0)|\hat{H}|\Psi(x,0)\rangle = p^2/2 + \sigma^2/2 + 1/(8\sigma^2)$. Therefore, we apply a gauge transform (17) of type (26) with

$$\bar{E}(t) = \frac{p^2}{2} + \frac{\sigma^2}{2} + \frac{1}{8\sigma^2}, \tag{31a}$$

$$g(x,t) = \int_0^t \bar{E}(\tau)d\tau, \tag{31b}$$

to Eq. (30) to get a new Hamiltonian $\hat{H}^*$ and the wave equation

$$i\frac{\partial\Psi'(x,t)}{\partial t} = -\frac{1}{2}\frac{\partial^2\Psi'(x,t)}{\partial x^2} + \left(\frac{x^2}{2} - \bar{E}(t)\right)\Psi'(x,t). \tag{32}$$

The new wave function $\Psi'(x,t) = \exp(ig(x,t))\Psi(x,t)$ features reduced temporal oscillations as illustrated in Fig. 1(b). Yet, spatial oscillations are still present.

B. Reducing spatial oscillations

Spatial oscillations of a wave function may be reduced by applying a gauge transform with the gauge function

$$g(\boldsymbol{x},t) = \int_0^t \bar{\boldsymbol{x}}(\tau)\cdot\frac{d}{d\tau}\left[m\frac{d\bar{\boldsymbol{x}}(\tau)}{d\tau} + q\boldsymbol{A}(\bar{\boldsymbol{x}}(\tau),\tau)\right]d\tau - \boldsymbol{x}\cdot\left[m\frac{d\bar{\boldsymbol{x}}(t)}{dt} + q\boldsymbol{A}(\bar{\boldsymbol{x}}(t),t)\right], \tag{33}$$

that is parametrized by some function $\bar{\boldsymbol{x}}(t)$. For the gauge transform (33), the new electromagnetic potentials (19) are given by

$$\boldsymbol{A}'(\boldsymbol{x},t) = \boldsymbol{A}(\boldsymbol{x},t) - \boldsymbol{A}(\bar{\boldsymbol{x}}(t),t) - \frac{m}{q}\frac{d\bar{\boldsymbol{x}}(t)}{dt}, \tag{34a}$$

$$\phi'(\boldsymbol{x},t) = \phi(\boldsymbol{x},t) + (\boldsymbol{x}-\bar{\boldsymbol{x}}(t))\cdot\frac{d}{dt}\left[\frac{m}{q}\frac{d\bar{\boldsymbol{x}}(t)}{dt} + \boldsymbol{A}(\bar{\boldsymbol{x}}(t),t)\right]. \tag{34b}$$

Plugging Eq. (33) into Eqs. (23a) and (23b) and using the relation

$$\langle \boldsymbol{p} \rangle(t) = m\frac{d\langle \boldsymbol{x} \rangle(t)}{dt} + q\langle \boldsymbol{A} \rangle(t) \tag{35}$$

between the mean canonical momentum $\langle \boldsymbol{p} \rangle(t)$ and the mean kinetic momentum $md\langle \boldsymbol{x} \rangle(t)/dt$, we get

$$\langle E' \rangle(t) = \langle E \rangle(t) + (\langle \boldsymbol{x} \rangle(t) - \bar{\boldsymbol{x}}(t)) \cdot \frac{d}{dt}\left[m\frac{d\bar{\boldsymbol{x}}(t)}{dt} + q\boldsymbol{A}(\bar{\boldsymbol{x}}(t),t) \right], \tag{36a}$$

$$\langle \boldsymbol{p}' \rangle(t) = \langle \boldsymbol{p} \rangle(t) - \left[m\frac{d\bar{\boldsymbol{x}}(t)}{dt} + q\boldsymbol{A}(\bar{\boldsymbol{x}}(t),t) \right]. \tag{36b}$$

We refer to the spectrum-guided integration in the *momentum domain* if $\Psi(\boldsymbol{x},t)$ is transformed into $\Psi'(\boldsymbol{x},t)$ by a gauge transform (17) with Eq. (33) and $\bar{\boldsymbol{x}}(t)$ such that the mean canonical momentum $\langle \boldsymbol{p}' \rangle(t)$ of the new system $\Psi'(\boldsymbol{x},t)$ vanishes and for that reason $\Psi'(\boldsymbol{x},t)$ has a smaller momentum band limit and exhibits spatial oscillations that have reduced frequencies compared to $\Psi(\boldsymbol{x},t)$. It is insightful to insert relation (35) between the canonical momentum and the kinetic momentum into Eq. (36b), which results in

$$\langle \boldsymbol{p}' \rangle(t) = m\frac{d}{dt}(\langle \boldsymbol{x} \rangle(t) - \bar{\boldsymbol{x}}(t)) + q[\langle \boldsymbol{A} \rangle(t) - \boldsymbol{A}(\bar{\boldsymbol{x}}(t),t)]. \tag{37}$$

As a consequence of Eq. (37), the spectrum-guided integration in the momentum domain can be realized by setting $\bar{\boldsymbol{x}}(t)$ equal to the trajectory of the corresponding classical system provided that quantum effects are small, that is, the classical trajectory equals $\langle \boldsymbol{x} \rangle(t)$ and $\langle \boldsymbol{A} \rangle(t) \approx \boldsymbol{A}(\langle \boldsymbol{x} \rangle(t),t)$. The expectation value of the energy (36a) will not be changed if $\bar{\boldsymbol{x}}(t)$ equals the center-of-mass motion of $\Psi(\boldsymbol{x},t)$. Note that if $\bar{\boldsymbol{x}}(t)$ does not strictly equal the center-of-mass trajectory $\langle \boldsymbol{x} \rangle(t)$, this just means that the reduction in the momentum band limit might be nonoptimal, but this will not introduce any errors.

In order to reduce spatial oscillations of the harmonic-oscillator wave function, one has to apply a gauge transform (17) of type (33) with

$$\bar{x}(t) = p\ \sin\ t, \tag{38a}$$

$$g(x,t) = \int_0^t \bar{x}(\tau)\frac{d^2\bar{x}(\tau)}{d\tau^2}d\tau - x\frac{d\bar{x}(t)}{dt}, \tag{38b}$$

to the wave equation (30). The function $\bar{x}(t)$ equals the classical trajectory related to the quantum harmonical oscillator (30). In Fig. 1(c) we show the oscillation pattern of the wave function $\Psi'(x,t) = \exp(ig(x,t))\Psi(x,t)$. Oscillations in the spatial domain have been reduced significantly.

C. Reducing temporal and spatial oscillations

It is possible to combine the gauge functions of the spectrum-guided integration in the energy domain (26) and spectrum-guided integration in the momentum domain (33) into a single gauge function

$$g(\boldsymbol{x},t) = \int_0^t \left\{ \bar{E}(\tau) + \bar{\boldsymbol{x}}(\tau) \cdot \frac{d}{d\tau}\left[m\frac{d\bar{\boldsymbol{x}}(\tau)}{d\tau} + q\boldsymbol{A}(\bar{\boldsymbol{x}}(\tau),\tau) \right] \right\} d\tau - \boldsymbol{x} \cdot \left[m\frac{d\bar{\boldsymbol{x}}(t)}{dt} + q\boldsymbol{A}(\bar{\boldsymbol{x}}(t),t) \right] \tag{39}$$

that reduces both temporal and spatial oscillations. The functions $\bar{E}(t)$ and $\bar{\boldsymbol{x}}(t)$ have to fulfill the conditions of the spectrum-guided integration in the energy domain and spectrum-guided integration in the momentum domain, respectively.

For our harmonic-oscillator example, we combine the gauge transforms (30) and (37) into the gauge function

$$\bar{E}(t) = \frac{p^2}{2} + \frac{\sigma^2}{2} + \frac{1}{8\sigma^2}, \tag{40a}$$

$$\bar{x}(t) = p\ \sin\ t, \tag{40b}$$

$$g(x,t) = \int_0^t \left(\bar{E}(\tau) + \bar{x}(\tau)\frac{d^2\bar{x}(\tau)}{d\tau^2} \right) d\tau - x\frac{d\bar{x}(t)}{dt} \tag{40c}$$

that reduces both temporal and spatial oscillations of the wave function as demonstrated in Fig. 1(d).

VI. WAVE EQUATIONS IN ACCELERATED FRAMES OF REFERENCE

The numerical propagation of wave functions is performed on spatial grids of finite size. In addition to the grid spacings Δx and Δt, the extent of the spatial grid limits the performance of numerical schemes for the propagation of wave functions too. On one hand, the grid has to be large enough to hold at all times all significant parts of the wave function. That is, the grid size has to ensure that the probability density outside of the grid is never significantly larger than zero. On the other hand, the grid should not be unnecessarily large in order to keep computational costs maintainable.

If a wave packet moves over distances that are large compared to the width of the wave packet then a static computational grid has to be much larger than the size of the wave packet. Consequently, the numerical propagation of fast moving wave packets is much more time demanding than the propagation of wave packets with a stationary center of mass. We can negotiate this problem by switching into an accelerated frame of reference.

A. Schrödinger equation in accelerated frames of reference

Let us consider two Schrödinger equation wave functions $\Psi(\boldsymbol{x},t)$ and $\Psi'(\boldsymbol{x},t)$ describing the same physical system in two different frames of reference that are shifted against each other by a time-dependent vector $\bar{\boldsymbol{x}}(t)$. These functions are related per construction by

$$\Psi'(\boldsymbol{x},t) = \hat{D}(\bar{\boldsymbol{x}}(t))\hat{U}_g\Psi(\boldsymbol{x},t), \tag{41}$$

where $\hat{U}_g$ denotes an arbitrary gauge transform (17) and $\hat{D}(\bar{\boldsymbol{x}}(t))$ denotes the unitary displacement operator that is generated by the canonical momentum operator $\hat{\boldsymbol{p}}$

$$\hat{D}(\bar{\boldsymbol{x}}(t)) = \exp\left[\frac{i}{\hbar}(-\bar{\boldsymbol{x}}(t)\cdot\hat{\boldsymbol{p}})\right] = \exp\left(\bar{\boldsymbol{x}}(t)\cdot\frac{\partial}{\partial \boldsymbol{x}}\right). \quad (42)$$

It is not difficult to show that the transform (41) changes the electromagnetic potentials but keeps the Schrödinger Hamiltonian (2) form invariant. That means Eq. (18) holds and the electromagnetic potentials transform as

$$\boldsymbol{A}'(\boldsymbol{x},t) = \boldsymbol{A}(\boldsymbol{x}+\bar{\boldsymbol{x}}(t),t) + \frac{1}{q}\frac{\partial g(\xi,t)}{\partial \xi}\bigg|_{\xi=\boldsymbol{x}+\bar{\boldsymbol{x}}(t)} + \frac{m}{q}\frac{d\bar{\boldsymbol{x}}(t)}{dt}, \quad (43a)$$

$$\phi'(\boldsymbol{x},t) = \phi(\boldsymbol{x}+\bar{\boldsymbol{x}}(t),t) - \frac{1}{q}\frac{\partial g(\boldsymbol{x}+\bar{\boldsymbol{x}}(t),\tau)}{\partial \tau}\bigg|_{\tau=t} - \left[\boldsymbol{A}(\boldsymbol{x}+\bar{\boldsymbol{x}}(t),t) + \frac{1}{q}\frac{\partial g(\xi,t)}{\partial \xi}\bigg|_{\xi=\boldsymbol{x}+\bar{\boldsymbol{x}}(t)}\right]\cdot\frac{d\bar{\boldsymbol{x}}(t)}{dt} - \frac{m}{2q}\left(\frac{d\bar{\boldsymbol{x}}(t)}{dt}\right)^2. \quad (43b)$$

However, the electromagnetic fields are not invariant because the operator $\hat{D}(\bar{\boldsymbol{x}}(t))\hat{U}_g$ does not represent a gauge transform. A transformation into an accelerated frame of reference causes inertial forces. The fields that correspond to the potentials (43) are given by

$$\boldsymbol{E}'(\boldsymbol{x},t) = \boldsymbol{E}(\boldsymbol{x}+\bar{\boldsymbol{x}}(t),t) - \frac{m}{q}\frac{d^2\bar{\boldsymbol{x}}(t)}{dt^2}, \quad (44a)$$

$$\boldsymbol{B}'(\boldsymbol{x},t) = \boldsymbol{B}(\boldsymbol{x}+\bar{\boldsymbol{x}}(t),t). \quad (44b)$$

The expectation values of the energy and the canonical momentum of the wave function in the accelerated frame of reference are given by

$$\langle E'\rangle(t) = \langle E\rangle(t) - \langle g_t\rangle(t) - (\langle \boldsymbol{p}\rangle(t) + \langle g_{\boldsymbol{x}}\rangle(t))\cdot\frac{d\bar{\boldsymbol{x}}(t)}{dt}, \quad (45a)$$

$$\langle \boldsymbol{p}'\rangle(t) = \langle \boldsymbol{p}\rangle(t) + \langle g_{\boldsymbol{x}}\rangle(t). \quad (45b)$$

1. Kramers-Henneberger transform

Transformation (41) is a generalization of the so-called Kramers-Henneberger transform [36]. The Kramers-Henneberger transform has proven to be useful for the numerical integration of the Schrödinger equation in dipole approximation as well as in the none-dipole regime [37]. For example, it had been utilized successfully to study various aspects of ionization dynamics [38], the suppression of ionization in superintense fields [39], as well as multiphoton ionization [40]. The Kramers-Henneberger transform reduces the energy band limit by switching into an accelerated frame of reference. As we will show, however, it does not reduce the energy band limit as much as possible in all physical setups.

Henneberger applied transformation (41) with

$$\bar{\boldsymbol{x}}(t) = -\int_0^t \frac{q}{m}\boldsymbol{A}(\tau)d\tau \quad (46a)$$

$$g(\boldsymbol{x},t) = \int_0^t \frac{q^2}{2m}\boldsymbol{A}(\tau)^2 d\tau \quad (46b)$$

to the Schrödinger equation in dipole approximation, where it is assumed that the vector potential does not depend on $\boldsymbol{x}$. The Hamiltonian is given by Eq. (2) with $\boldsymbol{A}(\boldsymbol{x},t)=\boldsymbol{A}(t)$. The Kramers-Henneberger transform changes the electromagnetic potentials into

$$\boldsymbol{A}'(t) = 0, \quad (47a)$$

$$\phi'(\boldsymbol{x},t) = \phi(\boldsymbol{x}+\bar{\boldsymbol{x}}(t),t), \quad (47b)$$

and the expectation values of the energy and the canonical momentum are given by

$$\langle E'\rangle(t) = \frac{\langle \boldsymbol{p}^2\rangle(t)}{2m} + q\langle\phi\rangle(t), \quad (48a)$$

$$\langle \boldsymbol{p}'\rangle(t) = \langle \boldsymbol{p}\rangle(t), \quad (48b)$$

where we have used the expression

$$\langle E\rangle(t) = \frac{\langle \boldsymbol{p}^2\rangle(t)}{2m} - \frac{q}{m}\boldsymbol{A}(t)\cdot\langle \boldsymbol{p}\rangle(t) + \frac{q^2}{2m}\boldsymbol{A}^2(t) + q\langle\phi\rangle(t) \quad (49)$$

for the mean energy in the original frame.

From Eq. (48), it follows that the Kramers-Henneberger transform does not affect the canonical momentum distribution. Yet, it reduces the energy band limit by shifting the energy spectrum. The mean energies (49) and (48a) differ by $-\frac{q}{m}\boldsymbol{A}(t)\cdot\langle \boldsymbol{p}\rangle(t)+\frac{q^2}{2m}\boldsymbol{A}^2(t)$, but the Kramers-Henneberger transform does not reduce the mean energy $\langle E'\rangle(t)$ to zero. Hence, it is not optimal. Only if $-\frac{q}{m}\boldsymbol{A}(t)\cdot\langle \boldsymbol{p}\rangle(t)+\frac{q^2}{2m}\boldsymbol{A}^2(t)$ is the dominating contribution to the mean energy (49) the Kramers-Henneberger transform will reduce the energy band limit significantly. If the scalar potential term $q\langle\phi\rangle(t)$ or the canonical momentum term $\langle \boldsymbol{p}^2\rangle(t)/(2m)$ in Eq. (49) is large, the Kramers-Henneberger transform may fail to reduce the energy band limit appreciably and the transformed wave function will exhibit high-frequency temporal oscillations as the original one does.

The failure of the Kramers-Henneberger transform may be illustrated by a system having an analytic solution, a particle in a harmonically oscillating homogeneous electric field with angular frequency ω, and amplitude ε [35]. The Schrödinger equation of this system reads in dimensionless units as

$$i\frac{\partial\Psi(x,t)}{\partial t} = \frac{1}{2}\left(-i\frac{\partial}{\partial x} - A(t)\right)^2\Psi(x,t), \quad (50a)$$

with

$$A(t) = \frac{\epsilon}{\omega}\sin(\omega t). \tag{50b}$$

Figure 2(a) visualizes the motion of the wave packet in the laboratory frame. The parameters of the initial Gaussian wave packet (29) are chosen such that a high initial canonical momentum propels the wave packet to the right and the electric field pushes the particle into the opposite direction. Because of the particle's high energy and its high momentum, the wave function oscillates strongly in time and space. Figure 2(b) shows the motion of the same particle in the Kramers-Henneberger frame

$$\bar{x}(t) = -\int_0^t \frac{\epsilon}{\omega}\sin(\omega\tau)d\tau, \tag{51a}$$

$$g(x,t) = \int_0^t \frac{1}{2}\frac{\epsilon^2}{\omega^2}\sin^2(\omega\tau)d\tau. \tag{51b}$$

In the Kramers-Henneberger frame, the canonical momentum equals the kinetic momentum and both are conserved quantities. The wave packet moves with constant velocity to the right. Because of the high initial momentum, the particle has also in the Kramers-Henneberger frame a high kinetic energy. Thus, the frequencies of time-spatial oscillations are reduced only slightly.

2. Schrödinger equation in the center-of-mass frame

We will circumvent the failure of the Kramers-Henneberger transform by transforming the Schrödinger equation into an accelerated frame of reference by Eq. (41), where the gauge transform $\hat{U}_g$ is generated by the gauge function of spectrum-guided integration (39). In the accelerated frame of reference, the new potentials (43) are given by

$$\boldsymbol{A}'(\boldsymbol{x},t) = \boldsymbol{A}(\boldsymbol{x}+\bar{\boldsymbol{x}}(t),t) - \boldsymbol{A}(\bar{\boldsymbol{x}}(t),t), \tag{52a}$$

$$\begin{aligned}\phi'(\boldsymbol{x},t) = {} & \phi(\boldsymbol{x}+\bar{\boldsymbol{x}}(t),t) + \boldsymbol{x}\cdot\frac{d}{dt}\left[\frac{m}{q}\frac{d\bar{\boldsymbol{x}}(t)}{dt} + \boldsymbol{A}(\bar{\boldsymbol{x}}(t),t)\right] \\ & - \frac{d\bar{\boldsymbol{x}}(t)}{dt}\cdot[\boldsymbol{A}(\boldsymbol{x}+\bar{\boldsymbol{x}}(t),t) - \boldsymbol{A}(\bar{\boldsymbol{x}}(t),t)] \\ & + \frac{m}{2q}\left(\frac{d\bar{\boldsymbol{x}}(t)}{dt}\right)^2 - \frac{\bar{E}(t)}{q}.\end{aligned} \tag{52b}$$

Note that in contrast to the Kramers-Henneberger transform, we do not require the dipole approximation $\boldsymbol{A}(\boldsymbol{x},t)=\boldsymbol{A}(t)$. Using Eqs. (39) and (45) and the relation (35) between the canonical momentum and the kinetic momentum, we find the expectation values of the energy and the canonical momentum

$$\begin{aligned}\langle E'\rangle(t) = {} & \langle E\rangle(t) - \bar{E}(t) - \frac{d\bar{\boldsymbol{x}}(t)}{dt}\cdot\left\{m\frac{d}{dt}(\langle\boldsymbol{x}\rangle(t) - \bar{\boldsymbol{x}}(t))\right. \\ & \left. + q[\langle\boldsymbol{A}\rangle(t) - \boldsymbol{A}(\bar{\boldsymbol{x}}(t),t)]\right\},\end{aligned} \tag{53a}$$

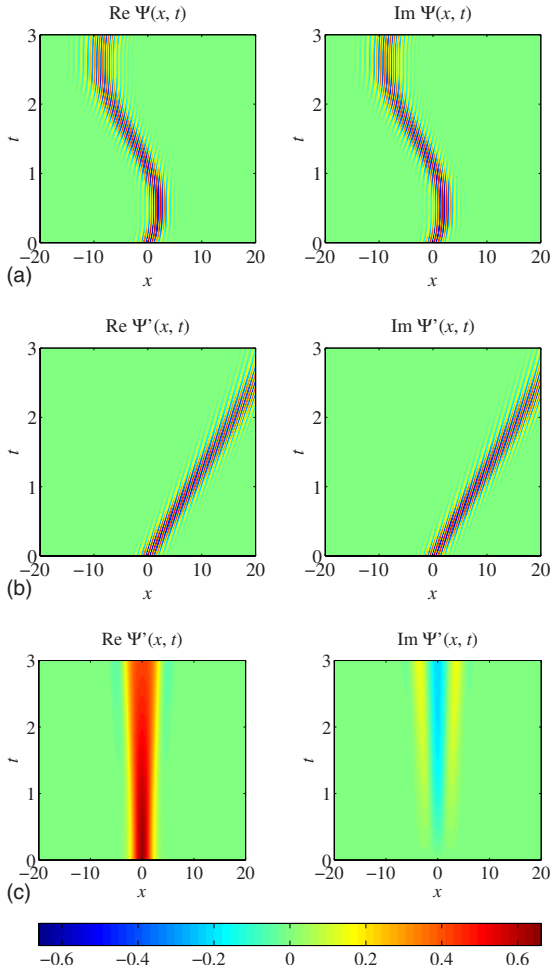

FIG. 2. (Color online) Motion of a wave packet in a harmonically oscillating homogeneous electric field (49) with field strength $\epsilon=16$ and frequency $\omega=1$. The figure compares the wave-packet's motion in the (a) laboratory frame, in the (b) Kramers-Henneberger frame, and in the (c) center-of-mass frame. The initial wave function in the laboratory frame is a Gaussian wave packet (29) of width $\sigma=1$ and momentum $p=8$. Figures display real (left) and imaginary (right) parts of the wave function.

$$\langle\boldsymbol{p}'\rangle(t) = m\frac{d}{dt}(\langle\boldsymbol{x}\rangle(t) - \bar{\boldsymbol{x}}(t)) + q[\langle\boldsymbol{A}\rangle(t) - \boldsymbol{A}(\bar{\boldsymbol{x}}(t),t)]. \tag{53b}$$

As a consequence of Eqs. (53), the expectation value of the energy $\langle E'\rangle(t)$ and the canonical momentum $\langle\boldsymbol{p}'\rangle(t)$ vanish if $\bar{\boldsymbol{x}}(t)$ equals the center-of-mass motion of $\Psi(\boldsymbol{x},t)$, if $\bar{E}(t)$ equals $\langle E\rangle(t)$ and if quantum effects are small, that means $\langle\boldsymbol{A}\rangle(t)\approx\boldsymbol{A}(\langle\boldsymbol{x}\rangle(t),t)$.

A transformation into an accelerated frame of reference that is determined by the center-of-mass motion of $\Psi(\boldsymbol{x},t)$ may be much more suitable to reduce time-spatial oscillations than the Kramers-Henneberger transform. For example, Fig. 2(c) shows the oscillation pattern of the wave function of a particle in a harmonically oscillating homogeneous electric field after transformation into the frame of reference that is determined by the classical energy

$$\bar{E}(t) = \frac{1}{2}\left(p - \frac{q\epsilon}{\omega}\sin(\omega t)\right)^2, \tag{54a}$$

the classical trajectory of the wave function $\Psi(\boldsymbol{x},t)$

$$\bar{x}(t) = \frac{q\epsilon}{\omega^2}(\cos(\omega t) - 1) + pt, \tag{54b}$$

and the gauge function

$$g(x,t) = \int_0^t \left(\bar{E}(\tau) + \bar{x}(\tau)\frac{d^2\bar{x}(\tau)}{d\tau^2}\right)d\tau - x\frac{d\bar{x}(\tau)}{d\tau}. \tag{54c}$$

In this frame, the center of mass is fixed and the wave-function's fast time-spatial oscillations virtually disappeared as shown in Fig. 2(c).

To sum up, the transformation of a quantum system into its rest frame in combination with the gauge transform (39), where $\bar{\boldsymbol{x}}(t)$ and $\bar{E}(t)$ are determined by the trajectory and the energy of the corresponding classical system fixes the center of mass and reduces high-frequency time-spatial oscillations. This transform may be interpreted as the removal of classical features from the motion of the wave function. However, the wave function in the center-of-mass frame $\Psi'(\boldsymbol{x},t)$ still comprises all quantum features, e.g., the broadening of a wave packet [see, for example, Fig. 2(c)].

B. Dirac equation in accelerated frames of reference

Two Dirac equation wave functions $\Psi(\boldsymbol{x},t)$ and $\Psi'(\boldsymbol{x},t)$ in two different frames of reference that are shifted against each other by $\bar{\boldsymbol{x}}(t)$ are related by a canonical transform (41) as in the case of Schrödinger wave functions. However, the shift operator $\hat{D}(\bar{\boldsymbol{x}}(t))$ has to take into account a Lorentz boost. For the Dirac wave functions, the operator $\hat{D}(\bar{\boldsymbol{x}}(t))$ reads as

$$\hat{D}(\bar{\boldsymbol{x}}(t)) = \exp\left(\frac{i}{\hbar}\frac{\omega}{c}\boldsymbol{n}\cdot\hat{\boldsymbol{N}}\right)\exp\left(-\frac{i}{\hbar}\bar{\boldsymbol{x}}(t)\cdot\hat{\boldsymbol{p}}\right). \tag{55}$$

The operator $\hat{\boldsymbol{N}}$ is defined as [27]

$$\hat{\boldsymbol{N}} = \frac{1}{2}(\hat{H}_0\boldsymbol{x} + \boldsymbol{x}\hat{H}_0), \tag{56}$$

where H_0 denotes the free particle Dirac Hamilton operator [operator (3) with $\varphi(\boldsymbol{x},t)=0$ and $\boldsymbol{A}(\boldsymbol{x},t)=0$] and the unit vector $\boldsymbol{n}$ and the rapidity ω are defined via

$$\frac{d\bar{\boldsymbol{x}}(t)}{dt} = c\boldsymbol{n}\tanh\omega. \tag{57}$$

The application of the operator $\hat{D}(\bar{\boldsymbol{x}}(t))\hat{U}_g$ to the Dirac equation (3) gives a new Dirac equation for $\Psi'(\boldsymbol{x},t)$ with transformed electromagnetic potentials. The operator (55) allows us to switch into the center-of-mass frame of $\Psi(\boldsymbol{x},t)$ in order to reduce the wave-function's high-frequency time-spatial oscillations as we did for the Schrödinger equation. However, we will not follow this path because the Lorentz boost mixes spatial coordinates with the coordinate of time. From this, it follows that an initial value problem for $\Psi(\boldsymbol{x},t)$ with an initial value function given at $t=0$ is transformed by Eq. (55) into an initial value problem for $\Psi'(\boldsymbol{x},t)$ with an initial value function given at some space-time slice. This is a kind of initial value problem that standard algorithms for the solution of time-dependent partial differential equations do not account for.

VII. CANONICAL TRANSFORMS AND NUMERICAL ALGORITHMS

In Secs. V and VI we demonstrated how a wave-function's high-frequency time-spatial oscillations may be reduced by canonical transforms. In this section, we are going to investigate how the reduction in time-spatial oscillations actually affects numerical algorithms.

A. Numerical solution of wave equations

In order to demonstrate the merits of canonical transforms for the numerical solution of quantum mechanical wave equations, we have implemented various numerical algorithms for the solution of the Schrödinger equation (2) and the Dirac equation (3). All these algorithms are based on the Cayley form of the time evolution operator (15b), a method that goes back to Goldberg *et al.* [4].

The Cayley form is a Padé approximant of the time evolution operator. Neglecting the time-ordering operator $\hat{T}$, we expand the time evolution operator into

$$\begin{aligned}\Psi(\boldsymbol{x},t+\Delta t) &= \hat{T}\exp\left(-\frac{i}{\hbar}\int_t^{t+\Delta t}\hat{H}(\tau)d\tau\right)\Psi(\boldsymbol{x},t)\\ &= \exp\left(-\frac{i}{\hbar}\int_t^{t+\Delta t}\hat{H}(\tau)d\tau\right)\Psi(\boldsymbol{x},t) + O(\Delta t^3)\\ &= \frac{1-\frac{i}{2\hbar}\int_t^{t+\Delta t}\hat{H}(\tau)d\tau}{1+\frac{i}{2\hbar}\int_t^{t+\Delta t}\hat{H}(\tau)d\tau}\Psi(\boldsymbol{x},t) + O(\Delta t^3).\end{aligned} \tag{58}$$

Up to terms of order Δt^3, the expansion (58) is equivalent to the implicit equation

$$\hat{D}_+\Psi(\boldsymbol{x},t+\Delta t) = \hat{D}_-\Psi(\boldsymbol{x},t), \tag{59a}$$

with

$$\hat{D}_\pm = 1 \pm \frac{i}{2\hbar}\int_t^{t+\Delta t}\hat{H}(\tau)d\tau. \tag{59b}$$

Mapping spatial coordinates to a regular grid, (59) gives a second-order accurate implicit time stepping scheme for the propagation of the initial value problem (1), $\Psi(\boldsymbol{x},0) = \Psi_0(\boldsymbol{x})$. The scheme (59) preserves the unitarity of the time evolution operator (15b) and is unconditionally stable.

In the spatially discrete version of Eq. (59), the operators $\hat{D}_\pm$ are matrices and Eq. (59a) is a system of linear equations that is solved very efficiently by iterative methods, i.e., Krylov subspace methods [41–45]. In particular, the conjugate

gradients squared method [42] and the biconjugate gradients stabilized method [44] have proven to be very efficient solvers for Eq. (59a). Iterative solvers construct a series of approximative solutions of the Eq. (59a) starting from the initial approximation $\Psi(\boldsymbol{x},t+\Delta t)\approx\Psi(\boldsymbol{x},t)$. The solver stops if a sufficient degree of accuracy is achieved. It is not required to solve Eq. (59a) to full machine precision, this will be a waste of computing time. However, the tolerable error in the solution of Eq. (59a) has to scale proportionally to Δt^3 as the error of the Cayley form does.

Krylov subspace methods are able to take advantage of the sparsity pattern of the coefficient matrix $\hat{D}_+$. It may be dense or sparse, depending on the way how spatial derivatives in the operator $\hat{D}_+$ are approximated. Finite difference approximations of differential operators result in sparse coefficient matrices, while pseudospectral methods [46] yield dense coefficient matrices. This makes the solution of the linear system (59a) computationally expensive. But pseudospectral methods may be superior to finite difference methods because they calculate spatial derivatives with "spectral accuracy," meaning the numerical error in the approximation of the spatial derivatives decreases superpolynomially in the number of grid points. The sparsity pattern also depends on the type of wave function and the dimension of the system. In the case of the one-dimensional Schrödinger equation with a second-order finite difference approximation of spatial derivatives, the matrix $\hat{D}_+$ is tridiagonal and the time stepping scheme (59) reduces to the well-known Crank-Nicolson scheme [4].

The implicit scheme (59) with finite difference approximations of differential operators and variants of this method [5,6,10] have been applied to the Schrödinger equation many times with great success. Here we apply the scheme (59) to the Dirac equation.

B. Numerical results

Spectrum-guided integration and integration in the center-of-mass frame are designed to reduce a wave-function's time-spatial oscillations. From a numerical point of view, propagating the transformed wave function $\Psi'(\boldsymbol{x},t)$ has two important advantages over propagating the original wave function $\Psi(\boldsymbol{x},t)$.

(i) If $\Psi(\boldsymbol{x},t)$ and $\Psi'(\boldsymbol{x},t)$ are propagated on a grid with the same time-spatial spacings Δt and Δx then the propagation of $\Psi'(\boldsymbol{x},t)$ will be more accurate than the propagation of the original wave function $\Psi(\boldsymbol{x},t)$.

(ii) If a particular degree of accuracy is required then $\Psi'(\boldsymbol{x},t)$ allows larger time-spatial spacings Δt and Δx than the propagation of the original wave function $\Psi(\boldsymbol{x},t)$. That means the spectrum-guided integration reduces computational costs.

These two important facts shall be illustrated by some examples.

1. Spectrum-guided integration

In our first example, we applied the spectrum-guided integration to the Schrödinger equation of the one-dimensional harmonic oscillator. We calculated the evolution of a Gaussian wave packet in a harmonic potential from $t=0$ to $t=\pi$ (a half period). The simulation was performed in the standard form (30) and in the form as obtained by spectrum-guided integration in the energy domain (32). The numerical results $\Psi_{\mathrm{num}}(x,t)$ and $\Psi'_{\mathrm{num}}(x,t)$ were compared to the exact solutions $\Psi(x,t)$ and $\Psi'(x,t)$ to determine the global errors of the modulus,

$$\Delta_{\mathrm{mod}}=\max_x\big||\Psi(x,t)|-|\Psi_{\mathrm{num}}(x,t)|\big|, \tag{60a}$$

as well as of the phase

$$\Delta_{\mathrm{phase}}=\max_{\overline{\Psi(x,t)}\cdot\Psi(x,t)>0.01}\big|\arg(\Psi(x,t)/\Psi_{\mathrm{num}}(x,t))\big|. \tag{60b}$$

For vector-valued wave functions, we take the maximum over all components and, for the calculation of the global phase error, we did not take into account regions of very small probability density, where phase errors can become very large but are of minor importance. Errors Δ'_{mod} and Δ'_{phase} of $\Psi'_{\mathrm{num}}(x,t)$ are defined analogously.

Figure 3 shows the effect of the spectrum-guided integration in the energy domain on the numerical errors (60a) and (60b) for $\Psi_{\mathrm{num}}(x,t)$ and $\Psi'_{\mathrm{num}}(x,t)$ as a function of the temporal step width Δt. The inset of Fig. 3 illustrates the shift of the energy spectrum that is caused by this technique. Errors for propagating a wave function over a finite time interval scale proportionally to Δt^2 because the Cayley form (58) neglects terms proportional to Δt^3. At fixed Δt, errors for $\Psi'(x,t)$ are about two orders of magnitude smaller than for $\Psi(x,t)$ due to the reduction in temporal oscillations by the spectrum-guided integration in the energy domain. Conse-

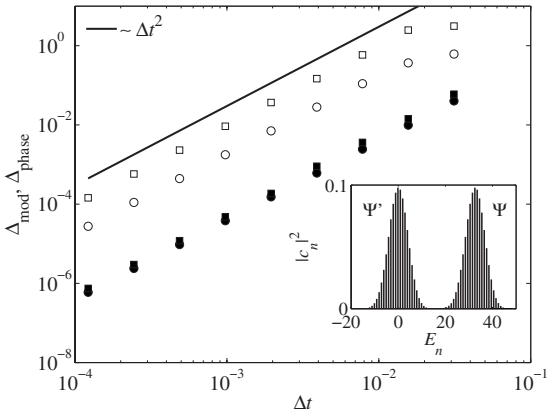

FIG. 3. Numerical errors (60a) and (60b) as a function of the temporal step width Δt for the motion of a Gaussian wave packet in a harmonic potential. The figure shows the maximal deviation of the modulus (circles) and the phase (squares) of the numerically calculated wave function at time $t=\pi$ (half period of the harmonic oscillator) from the exact solution. Open symbols correspond to $\Psi(x,t)$; full symbols correspond to $\Psi'(x,t)$. The wave function was initially given by a Gaussian wave packet (29) of width $\sigma=1$ and initial momentum $p=8$. The inset shows the discrete energy spectra of $\Psi(x,t)$ and $\Psi'(x,t)$; c_n denotes the expansion coefficient related to the nth eigenfunction.

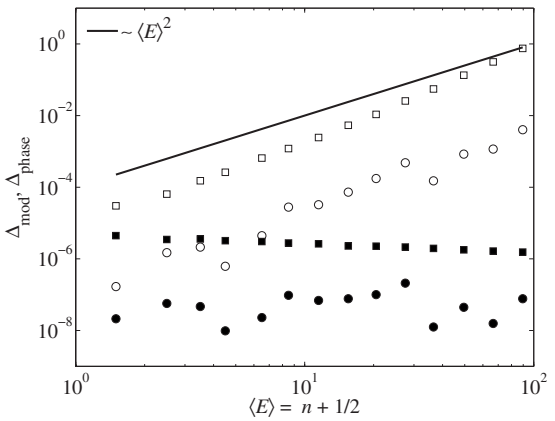

FIG. 4. Numerical errors (60a) and (60b) as a function of the mean energy $\langle E\rangle$ for the motion of a wave packet (61) in a harmonic potential. The figure shows the maximal deviation of the modulus (circles) and the phase (squares) of the numerically calculated wave function at time $t=\pi$ (half period of the harmonic oscillator) from the exact solution. Open symbols correspond to $\Psi(x,t)$; full symbols correspond to $\Psi'(x,t)$.

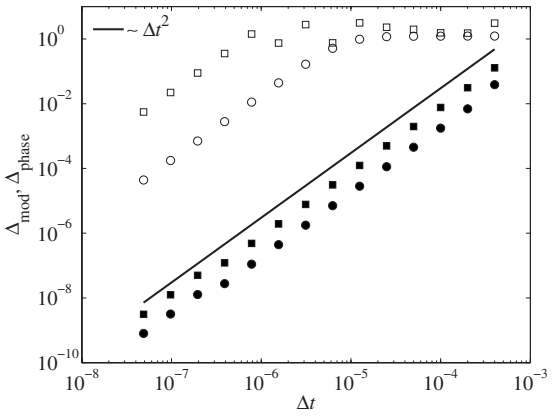

FIG. 5. Numerical errors (60a) and (60b) as a function of the temporal step width Δt for the motion of a free Gaussian Dirac wave packet. Meaning of the symbols as in Fig. 3.

quently, if a fixed accuracy for propagating a wave function over a given time interval is demanded then the gauge transformed wave function requires a smaller number of time steps than the original wave function.

The Shannon sampling theorem states that the higher the energy of a system, the smaller the step size Δt that a numerical algorithm requires. Spectrum-guided integration translates a wave function into a system with zero mean energy. Therefore, the step size for the new wave function is limited only by the width of the energy distribution. Figure 4 shows how numerical errors scale as a function of the mean energy $\langle E\rangle$ of $\Psi(x,t)$ if the width of the energy distribution is fixed. Here, we have simulated a wave packet in a harmonic potential (30) with the initial condition

$$\Psi(x,0) = \frac{\sqrt{6}}{3}[\psi_{n-1}(x)/2 + \psi_n(x) + \psi_{n+1}(x)/2], \qquad (61)$$

where $\psi_n(x)$ denotes a normalized eigenfunction of the harmonic oscillator with energy $E=n+1/2$. Numerical errors for simulating $\Psi(x,t)$ scale quadratically in $\langle E\rangle=n+1/2$. The quadratic scaling behavior is a result of neglecting third-order terms in the Cayley form (58). However, if the spectrum-guided integration with the gauge function $g(x,t)=(n+1/2)t$ is applied errors are independent of the energy $\langle E\rangle$. Spectrum-guided integration in the energy domain is particularly useful if the width of the energy distribution is small compared to the mean energy.

This scenario arises frequently in relativistic wave equations, e.g., the Dirac equation (3), due to the relativistic rest mass energy. Figure 5 shows data analogous to Fig. 3 for the simulation of a free one-dimensional Dirac wave packet with initial momentum $p=25$ from $t=0$ to $t=0.04$ (in dimensionless units). The Shannon sampling theorem requires a temporal step width Δt that is smaller than the inverse energy of the system. This means an accurate numerical propagation of $\Psi(x,t)$ requires $\Delta t \ll 1/\sqrt{c^4+p^2c^2} \approx 5\times 10^{-5}$. Our numerical results in Fig. 5 confirm this upper bound on Δt. However, the spectrum-guided integration in the momentum domain allows to increase the temporal step width by several orders of magnitude. Here, spectrum-guided integration was realized by a gauge function $g(x,t)=t\sqrt{c^4+p^2c^2}$.

Spectrum-guided integration in the momentum domain affects numerical errors in a similar way as the spectrum-guided integration in the energy domain does. However, it allows for larger spatial step widths if a fixed degree of accuracy is required. This is illustrated, once more, by the simulation of a Gaussian wave packet in a harmonic potential by the implicit scheme (59) applying a second-order accurate finite difference formula to approximate spatial derivatives in $\hat{D}_+$. Therefore, global errors (60a) and (60b) scale quadratically in Δx^2. The gauge function of the spectrum-guided integration in the momentum domain for this system is given by Eqs. (38). It reduces errors by about an order of magnitude for the parameters as chosen here, see Fig. 6.

2. Accelerated frames of reference

The effect of a wave-function's transformation into an accelerated frame of reference on numerical algorithms is exemplified by solving the Schrödinger equation (50) numerically for a particle in a harmonically oscillating homogeneous electric field [35]. We propagated this system in the laboratory frame, in the Kramers-Henneberger frame, as well as in the center-of-mass frame applying a Crank-Nicolson code with the same temporal and spatial step sizes $\Delta t=0.001$ and $\Delta x=0.01$. For the parameter set and the initial condition we have chosen here, we found that the propagation of the wave function is carried out most accurately in the center-of-mass frame [Eqs. (54)]. In fact, in the center-of-mass frame, the numerical error is reduced by more than three orders of magnitude compared to a calculation in the laboratory frame or the Kramers-Henneberger frame (51), as shown in Fig. 7.

C. Computational performance

We demonstrated in the previous sections how canonical transforms can be utilized to allow larger temporal and spa-

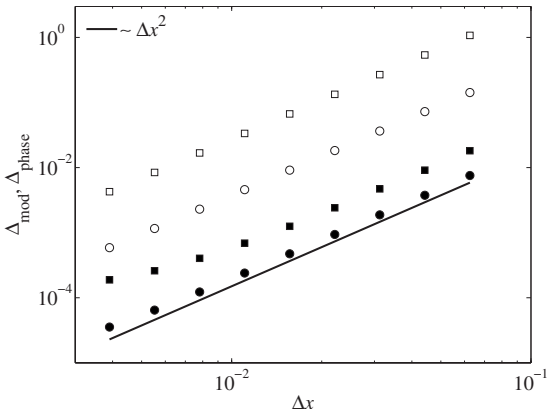

FIG. 6. Numerical errors (60a) and (60b) as a function of the spatial step width Δx for the motion of a Gaussian wave packet in a harmonic potential. The figure shows the maximal deviation of the modulus (circles) and the phase (squares) of the numerically calculated wave function at time $t=2\pi$ (full period of the harmonic oscillator) from the exact solution. Open symbols correspond to $\Psi(x,t)$; full symbols correspond to $\Psi'(x,t)$. The wave function was initially given by a Gaussian wave packet (29) of width $\sigma=1$ and initial momentum $p=7$.

tial step sizes in the numerical solution of quantum mechanical wave equations. In Sec. III we motivated the desire for large temporal and spatial steps by a possible reduction in the overall computational cost. However, it is not self-evident that an increase in temporal and spatial step sizes will actually reduce the overall computational cost. For example, on one hand, spectrum-guided integration in the energy domain allows to increase the temporal step size and reduces the number temporal steps that is required to cover a given time interval. On the other hand, spectrum-guided integration requires a modification of the electromagnetic potentials and changes thereby the Hamiltonian. This affects the condition

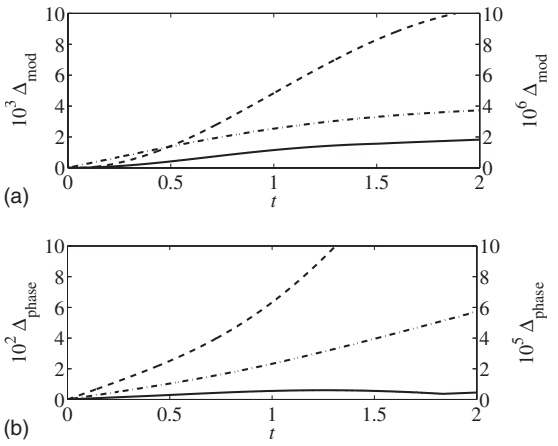

FIG. 7. Numerical errors (60a) and (60b) as a function of time t at fixed Δt and Δx for the motion of a Gaussian wave packet in a harmonically oscillating potential. Dashed lines and left scale correspond to the wave function $\Psi(x,t)$ in the laboratory frame, dot-dashed lines and left scale correspond to the wave function $\Psi'(x,t)$ in the Kramers-Henneberger frame, and full lines and right scale correspond to $\Psi'(x,t)$ in the center-of-mass frame. Same parameters and initial conditions as in Fig. 2.

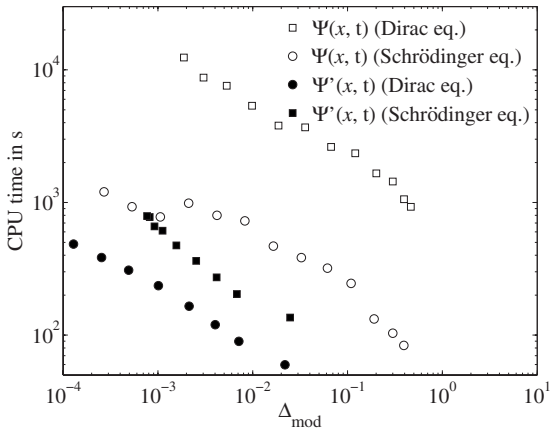

FIG. 8. CPU time as a function of the numerical accuracy for the simulation of free wave packets with and without the application of the spectrum-guided integration in the energy domain.

of the matrix $\hat{D}_+$ and the computational cost (number of iterations) of solving Eqs. (59) to a sufficient level of accuracy by iterative methods.

In fact, we observe that for the same values of Δt and Δx the iterative solution of the linear system [Eqs. (59)] (to the same degree of precision) requires often more iterations for the system obtained from a canonical transform than the original system. Nevertheless, the overall computational cost may be reduced considerably by canonical transforms, as illustrated in Fig. 8. This figure shows the CPU time that is required to simulate the motion of a free two-dimensional Gaussian wave packet with a high initial momentum $p_0=40$ over a time interval of length 0.025. Different levels of accuracy are obtained by varying the temporal step width. In dimensionless units, the free motion is governed by the Schrödinger equation

$$i\frac{\partial\Psi(\boldsymbol{x},t)}{\partial t}=-\frac{1}{2}\frac{\partial^2\Psi(\boldsymbol{x},t)}{\partial\boldsymbol{x}^2} \tag{62}$$

and if relativistic effects are taken into account by the Dirac equation

$$i\frac{\partial\Psi(\boldsymbol{x},t)}{\partial t}=c\boldsymbol{\alpha}\cdot\left(-i\hbar\frac{\partial\Psi(\boldsymbol{x},t)}{\partial\boldsymbol{x}}\right)+c^2\beta\Psi(\boldsymbol{x},t). \tag{63}$$

A gauge transform with the gauge function of the spectrum-guided integration in the energy domain

$$g(\boldsymbol{x},t)=\begin{cases}tp_0^2/2 & \text{for the Schrödinger equation}\\ t\sqrt{c^4+c^2p_0^2} & \text{for the Dirac equation}\end{cases} \tag{64}$$

leads to wave equations for $\Psi'(\boldsymbol{x},t)$ that are much better suited for the numerical propagation than the original ones. In the case of the Schrödinger equation, spectrum-guided integration has reduced the computing time by about an order of magnitude and for the Dirac equation by almost two orders of magnitude as shown in Fig. 8.

Further numerical experiments not shown here confirm that both spectrum-guided integration in the momentum domain and transformations into accelerated frames of reference reduce the CPU time similarly to spectrum-guided integration in the energy domain. The precise amount of computing time reduction depends on the kind of physical problem under investigation and to some degree on implementation details of the implicit scheme (59), e.g., how partial differences are approximated and what kind of iterative solver is applied. The simulation results in Fig. 8 have been obtained by a two-dimensional pseudospectral code for the Schrödinger equation and by a two-dimensional fourth-order finite difference scheme in the case of the Dirac equation.

We also benchmarked our Dirac solver to another state-of-the-art Dirac solver that is based on the split operator method [47]. The split operator method has a computational advantage over the implicit scheme (59) because, as an explicit method, it does not require the solution of a linear system in each time step. However, it does not take advantage of spectrum-guided integration in the energy domain (see Sec. VII D). Our simulation experiments yield that the combination of spectrum-guided integration in the energy domain and the implicit scheme (59) outperform the split operator method by about an order of magnitude.

D. Algorithmic considerations

In Sec. V we introduced the spectrum-guided integration as a technique that is able to boost the performance of numerical integration methods for quantum mechanical wave equations without taking into account any algorithmic specific considerations. For the implicit propagation scheme (59), we demonstrated in Secs. VII B and VII C the benefits of spectrum-guided integration and we believe that the spectrum-guided integration assists many other propagation schemes in a similar way. However, propagation schemes based on operator splitting techniques may not benefit from spectrum-guided integration in the energy domain.

Splitting techniques, as, for example, alternating-direction-implicit-like methods [5,48] and the split operator method [9], approximate the time evolution operator (15b) by a product of n operators $\hat{U}_i$, such that the short-time evolution is given by

$$\Psi(\boldsymbol{x},t+\Delta t)=\hat{U}_{\hat{H}}\Psi(\boldsymbol{x},t)\approx\hat{U}_n\cdots\hat{U}_2\hat{U}_1\Psi(\boldsymbol{x},t). \quad (65)$$

The overall numerical error of the product operator $\hat{U}_n\cdots\hat{U}_2\hat{U}_1$ is the sum of the individual errors of the respective operators $\hat{U}_i$. The larger the phase change induced by the application of $\hat{U}_i$, the larger the numerical error that is associated with this operator.

Spectrum-guided integration in the energy domain is designed to make the phase change between the wave functions at times t and $t+\Delta t$ small. However, phase changes between intermediate products, e.g., $\hat{U}_1\Psi(\boldsymbol{x},t)$ and $\hat{U}_2\hat{U}_1\Psi(\boldsymbol{x},t)$, may be large even if the overall phase change generated by $\hat{U}_n\cdots\hat{U}_2\hat{U}_1$ is small. Consequently, the overall numerical error generated by the successive application of $\hat{U}_i$ may be large and, therefore, splitting techniques are not able to take advantage of spectrum-guided integration in the energy domain if intermediate operators $\hat{U}_i$ cause large phase shifts. Note that spectrum-guided integration in the momentum domain does not suffer from these kinds of algorithm specific limitations of splitting methods.

VIII. CONCLUSIONS

As a consequence of the Shannon sampling theorem, the performance of algorithms for the numerical solution of quantum mechanical wave equations is fundamentally limited by the wave-function's energy spectrum as well as its momentum spectrum. If the wave function is (approximately) band limited in the momentum domain to $\tilde{p}$ and (approximately) band limited in the energy domain to $\tilde{E}$ then the distance between spatial grid points as well as the distance between temporal grid points are limited to $\Delta x \leq \hbar\pi/\tilde{p}$ and $\Delta t \leq \hbar\pi/\tilde{E}$, respectively. However, the energy and momentum spectra depend on the Hilbert-space representation of the quantum mechanical system. Canonical transforms provide transitions between different Hilbert spaces. Therefore, finding a canonical transform that leads to a representation where the wave function has a low energy band limit and a low momentum band limit is the key to the efficient numerical solution of quantum mechanical wave equations.

In this contribution, we have proposed techniques to reduce a wave-function's energy band limit and its momentum band limit. We introduced spectrum-guided integration and considered the transition into accelerated frames of reference. Spectrum-guided integration as well as the transition into a system's rest frame allow to expand the distance between time-spatial grid points and boost the performance of algorithms for the numerical solution of wave equations by up to several orders of magnitude. Both transformations are very generic approaches and do not rely on special features of a quantum mechanical system; these techniques may be applied to any quantum wave equation in Schrödinger form.

[1] S. Flügge, *Practical Quantum Mechanics*, Classics in Mathematics (Springer, New York, 1994).
[2] V. G. Bagrov and D. Gitman, *Exact Solutions of Relativistic Wave Equations*, Mathematics and Its Applications Vol. 39 (Springer, New York, 1990).
[3] G. E. Kimball and G. H. Shortley, Phys. Rev. **45**, 815 (1934).
[4] A. Goldberg, H. M. Schey, and J. L. Schwartz, Am. J. Phys. **35**, 177 (1967).
[5] I. Galbraith, Y. S. Ching, and E. Abraham, Am. J. Phys. **52**, 60 (1984).

[6] N. Watanabe and M. Tsukada, Phys. Rev. E **62**, 2914 (2000).
[7] A. Askar and A. S. Cakmak, J. Chem. Phys. **68**, 2794 (1978).
[8] D. Kosloff and R. Kosloff, J. Comput. Phys. **52**, 35 (1983).
[9] M. D. Feit, J. A. Fleck, Jr., and A. Steiger, J. Comput. Phys. **47**, 412 (1982).
[10] W. van Dijk and F. M. Toyama, Phys. Rev. E **75**, 036707 (2007).
[11] T. Iitaka, Phys. Rev. E **49**, 4684 (1994).
[12] A. D. Bandrauk and H. Shen, Chem. Phys. Lett. **176**, 428 (1991).
[13] A. D. Bandrauk and H. Shen, J. Chem. Phys. **99**, 1185 (1993).
[14] I. P. Omelyan, I. M. Mryglod, and R. Folk, Phys. Rev. E **66**, 026701 (2002).
[15] I. P. Omelyan, I. M. Mryglod, and R. Folk, Comput. Phys. Commun. **151**, 272 (2003).
[16] T. N. Rescigno and C. W. McCurdy, Phys. Rev. A **62**, 032706 (2000).
[17] B. I. Schneider, L. A. Collins, and S. X. Hu, Phys. Rev. E **73**, 036708 (2006).
[18] X. Guan, K. Bartschat, and B. I. Schneider, Phys. Rev. A **77**, 043421 (2008).
[19] M. Ndong, H. Tal-Ezer, R. Kosloff, and C. P. Koch, J. Chem. Phys. **130**, 124108 (2009).
[20] S. Succi, Phys. Rev. E **53**, 1969 (1996).
[21] S. Succi, *Cellular Automata*, Lecture Notes in Computer Science Vol. 2493 (Springer, New York, 2002), pp. 114–122.
[22] S. Palpacelli and S. Succi, Phys. Rev. E **75**, 066704 (2007).
[23] C. Leforestier *et al.*, J. Comput. Phys. **94**, 59 (1991).
[24] J. W. Braun, Q. Su, and R. Grobe, Phys. Rev. A **59**, 604 (1999).
[25] G. R. Mocken and C. H. Keitel, J. Comput. Phys. **199**, 558 (2004).
[26] W. Bao and L. Yang, J. Comput. Phys. **225**, 1863 (2007).
[27] B. Thaller, *The Dirac Equation*, Texts and Monographs in Physics (Springer, New York, 1992).
[28] H. Feshbach and F. Villars, Rev. Mod. Phys. **30**, 24 (1958).
[29] A. J. Jerri, Proc. IEEE **65**, 1565 (1977).
[30] A. Borzì and E. Decker, J. Comput. Appl. Math. **193**, 65 (2006).
[31] S. A. Chin, Phys. Rev. E **76**, 056708 (2007).
[32] M. Born, W. Heisenberg, and P. Jordan, Z. Phys. **35**, 557 (1926).
[33] M. Jammer, in *The Conceptual Development of Quantum Mechanics*, History of Modern Physics Series 1800–1950 Vol. 12, 2nd ed. (American Institute of Physics, New York, 1989).
[34] I. P. Omelyan, Phys. Rev. E **78**, 026702 (2008).
[35] K. Fan, Y. Zheng, W. Ren, and S. Ding, Int. J. Quantum Chem. **107**, 1355 (2007).
[36] W. C. Henneberger, Phys. Rev. Lett. **21**, 838 (1968).
[37] M. Førre, S. Selstø, J. P. Hansen, and L. B. Madsen, Phys. Rev. Lett. **95**, 043601 (2005).
[38] V. C. Reed and K. Burnett, Phys. Rev. A **42**, 3152 (1990).
[39] V. C. Reed, P. L. Knight, and K. Burnett, Phys. Rev. Lett. **67**, 1415 (1991).
[40] I. A. Ivanov and A. S. Kheifets, J. Phys. B **38**, 2245 (2005).
[41] Y. Saad, *Iterative Methods for Sparse Linear Systems* (SIAM, Philadelphia, 2003).
[42] P. Sonneveld, SIAM (Soc. Ind. Appl. Math.) J. Sci. Stat. Comput. **10**, 36 (1989).
[43] R. W. Freund and N. M. Nachtigal, Numer. Math. **60**, 315 (1991).
[44] H. A. van der Vorst, SIAM (Soc. Ind. Appl. Math.) J. Sci. Stat. Comput. **13**, 631 (1992).
[45] T. Sogabe and S.-L. Zhanga, J. Comput. Appl. Math. **199**, 297 (2007).
[46] J. P. Boyd, *Chebyshev and Fourier Spectral Methods*, 2nd ed. (Dover, New York, 1999).
[47] G. R. Mocken and C. H. Keitel, Comput. Phys. Commun. **178**, 868 (2008).
[48] D. W. Peaceman and H. H. Rachford, Jr., J. Soc. Ind. Appl. Math. **3**, 28 (1955).